THE JOURNAL OF PHYSICAL CHEMISTRY A

Article

pubs.acs.org/JPCA

Quasiclassical Trajectory Study of the C(^{1}D) + H_2 → CH + H Reaction on a New Global *ab Initio* Potential Energy Surface

Ying Wu,[†,‡] Chunfang Zhang,[†,‡] Jianwei Cao,*[,†] and Wensheng Bian*[,†]

[†]Beijing National Laboratory for Molecular Sciences, Institute of Chemistry, Chinese Academy of Sciences, Beijing 100190, China

[‡]University of Chinese Academy of Sciences, Beijing 100049, China

ABSTRACT: Quasiclassical trajectory (QCT) calculations have been performed on a new global *ab initio* potential energy surface (PES) for the singlet ground state ($1^1A'$) of the CH_2 reactive system. Our new PES can give a very good description of the well and asymptote regions, and particularly regions around conical intersections (CIs) and of van der Waals (vdW) interactions. The integral cross sections, differential cross sections, and product rovibrational state distributions for the C(^{1}D) + H_2 → CH + H reaction have been investigated in a wide range of collision energies. The present integral cross sections are much larger than the previous QCT results at low collision energies, which can be attributed to the differences of the PESs in the regions around the CIs and vdW complexes. The thermal rate coefficients in the temperature range 200−1500 K have also been calculated and very good agreement with experiment is obtained.

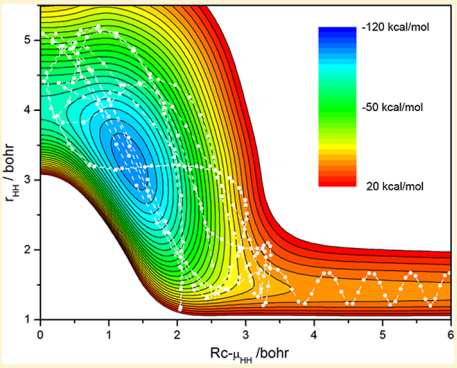

1. INTRODUCTION

The C(^{1}D) + H_2 → CH + H reaction is regarded as a prototype for the complex-forming insertion processes, and it is relevant to numerous organic reactions where a carbon atom is inserted into C−H and C−C bonds.[1] Consequently, the title reaction has been the subject of considerable experimental and theoretical works, which have been reviewed illuminatingly and extensively in the literature.[2−6]

Experimentally, a number of kinetic and dynamical studies on the title reaction and its isotopic variants have been reported,[2,7−16] including several crossed molecular-beam (CMB) experiments.[2,13−16] In particular, Liu[2] reported the excitation function for the C(^{1}D) + D_2 reaction, Bergeat et al.[13] measured the product angular and time-of-flight (TOF) distributions for the C(^{1}D) + H_2 reaction at the collision energy of 1.86 kcal/mol, and Balucani et al.[14] obtained the product angular and velocity distributions at two collision energies of 7.8 and 16.0 kJ/mol for the C(^{1}D) + H_2 reaction. As for the thermal rate coefficient, the most recent measurements have been published by Sato et al.,[12] who reported the value of $(2.0 \pm 0.6) \times 10^{-10}$ cm^3 molecule^{-1} s^{-1} at the temperature of 298 K.

Theoretically, Bussery-Honvault et al. constructed a global *ab initio* potential energy surface (PES) (Bussery-Honvault−Honvault−Launay (BHL)) for the singlet ground state ($1^1A'$).[17] After that, the *ab initio* data for the BHL PES were refitted with the reproducing kernel Hilbert space (RKHS) method to remove some spurious features of the original BHL PES.[18] Quantum mechanical (QM)[17,19−25] and quasiclassical trajectory (QCT)[4,14−16,18,24−27] methods were applied to investigate the title reaction using the aforementioned PESs, including several combined experimental and theoretical studies.[13−16] In 2009, Varandas and co-workers[28] developed a double many-body expansion (DMBE) PES for the $1^1A'$ state of the CH_2 system by fitting accurate *ab initio* energies that have been semiempirically corrected by the DMBE scaled-external-correlation method. On the basis of the DMBE PES, Varandas and co-workers[29] carried out QCT calculations and the calculated cross sections, rate coefficients, and branching ratios were found to agree well with the available experimental data. Most recently, Sun et al.[30] reported accurate quantum wave packet calculations for the title reaction on a new global *ab initio* PES; the computed rate coefficients are in good agreement with experiment, and the obtained CH_2 vibrational energy levels agree well with the experimental data, which are superior to those obtained on the BHL PES.

The QCT method has been widely used to study and interpret the features of reaction dynamics over the decades.[31−33] Extensive comparisons have indicated that the QCT method can give good approximation to the scattering dynamical properties,[4,34] especially the highly averaged ones such as the total cross section and rate coefficient. However, it suffers from its approximate nature and inherent limitations in describing the purely quantum mechanical effects, such as tunneling, zero-point energy (ZPE) and resonance. To fix the ZPE problem, Gaussian binning (GB) type approaches have been proposed.[35−37] Unlike the conventional histogram binning (HB) approach which rounds the final product vibrational quantum number to the nearest integer, the GB method assigns each trajectory emerging in the product channel to a weight defined by a Gaussian function centered at the product vibrational energy level. The GB approach was first used for an insertion reaction by Aoiz and co-workers,[25] which

Received: May 5, 2014
Published: May 30, 2014

   dx.doi.org/10.1021/jp504411j | *J. Phys. Chem. A* 2014, 118, 4235−4242

has yielded calculational results in preferable agreement with the QM ones, such as the vibrational branching ratios and product rotational distributions.

In the present work, we performed detailed QCT calculations on a new global *ab initio* PES for the singlet ground state ($1^1A'$) of the CH_2 reactive system. Various dynamical quantities and thermal rate coefficients for the title reaction are obtained. This article is organized as follows. In section 2, our PES is introduced, and the methodology and computational details for the QCT studies are elucidated. The results of QCT calculations are presented and discussed in section 3. Finally, a summary is given in section 4.

2. CALCULATION DETAILS

Potential Energy Surface. The PES used in this work is a newly constructed global *ab initio* PES of the singlet ground state ($1^1A'$) of the CH_2 reactive system. Energy points covering various PES regions for the $1^1A'$ state are calculated with the internally contracted multireference configuration interaction (*ic*MRCI)[38,39] approach using the MOLPRO suite[40] of *ab initio* programs. The five-reference-state *ic*MRCI calculations are performed to describe most of the correlation energy, whereas additional correlation energy due to higher excitations is included by the Davidson correction (+Q). The Dunning's correlation consistent quadruple-ζ basis augmented by diffuse functions (aug-cc-pVQZ)[41,42] is chosen, and the active space consists of six electrons distributed among seven orbitals. Totally, around 9300 symmetry unique *ab initio* energy points are used in the global fit. The fit of the PES is based on the many-body expansion,[43−48] and the analytical functions proposed by Aguado and Paniagua (AP)[48] are used in the two-body and three-body expansions. The AP function cannot give an accurate description of the region around conical intersection (CI), so the regions around CIs are fitted separately with a modified AP function based upon a polynomial fitted to the CI seam and then merged with the well and asymptote regions using switching functions to produce the global surface. The root-mean-square (rms) error of the global fit is 0.349 kcal/mol for energy points ranging from the global minimum up to 20 kcal/mol above the $C(^1D) + H_2$ asymptote, though the fitting errors in dynamically important regions are much lower, because energy points in these regions are given very high weights in the fitting process, which improves the quality of the surface. Further details about the *ab initio* calculations and the fit, as well as various properties of the fitted PES, will be given in a separate publication.[49]

The QCT calculations require the PES to evaluate the potential energy gradients at arbitrary geometries in the configuration space accurately and quickly, which is crucial for the total energy conservation in numerical integration as well as the computational efficiency. In most configuration regions, our PES could meet this requirement easily, because we have derived analytic gradient expressions for the purpose of programming; however, the use of some available switching functions may lead to problems due to discontinuity of the first derivatives at some specific points. Thus, in the construction of our surface, the forms of those switching functions used to combine different regions are carefully chosen to make sure that they always have continuous first derivatives and are permutationally invariant. The resulting global surface is very smooth and can offer a fast evaluation of the analytic gradients, which ensures the stability of the trajectories and significantly speeds up the large-scale QCT calculations.

The present PES can give a very good description of the well, asymptote, and particularly the CI and van der Waals (vdW) regions. In the $C + H_2$ collinearly attacking approach direction, our surface shows a high barrier caused by the CI between the $1^1A'$ and $2^1A'$ states, the height of which is 12.39 kcal/mol (All the energies in this article are relative to the $C(^1D) + H_2$ asymptote), in very good agreement with our *ab initio* value of 12.69 kcal/mol. Meanwhile, in the linear H−CH dissociation direction, our surface has another barrier caused by the CI between the $1^1A'$ and $2^1A'$ states with the height of 9.07 kcal/mol, which is rather close to our *ab initio* value of 9.29 kcal/mol, but much higher than that (4.43 kcal/mol) of the BHL surface. In addition, the locations of the above CIs on our surface are also in very good agreement with our *ab initio* results. For instance, the location of the minimum energy crossing point of the linear CHH CI is at R_{CH} = 2.504 bohr and R_{HH} = 1.818 bohr on our surface, which is closer to the *ab initio* values (R_{CH} = 2.51 bohr and R_{HH} = 1.81 bohr) than those (R_{CH} = 2.55 bohr and R_{HH} = 1.85 bohr) on the DMBE surface. Furthermore, the present PES has a very good description of the vdW interactions in the entrance and exit valleys, which are shown to have a significant effect on the reaction dynamics by more and more evidence.[33,47] We find three vdW complexes, with one at a linear C−HH geometry in the entrance channel, and two in the exit channel at linear CH−H and HC−H geometries, respectively. We calculate more than 100 *ab initio* points around each vdW extremal point, and then fit these *ab initio* points with great care; our fitting basically reproduces our *ab initio* calculational values of the location and energy for each vdW complex. For example, in the entrance channel, our surface supports a linear C−HH vdW complex with an energy of −0.294 kcal/mol, which is quite close to our *ab initio* energy of −0.306 kcal/mol, whereas the DMBE PES has a much lower value (−0.8 kcal/mol) for the vdW complex.

A typical contour plot is illustrated in Figure 1, in which the barrier caused by the linear CHH CI (between $1^1A'$ and $2^1A'$) (right), the barrier caused by the linear HCH CI (between $1^1A'$

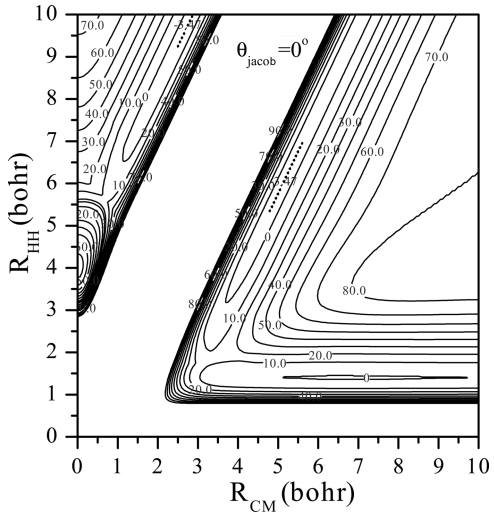

Figure 1. Contour plot of the present PES as a function of the Jacobi coordinates R_{CM} (the radial distance between the C atom and the center-of-mass of the two H atoms) and R_{HH} (the separation between the two H atoms) with the Jacobi angle (the angle between R_{CM} and R_{HH}) fixed at 0.0°. The contour spacing is 10.0 kcal/mol, with the energy of the $C(^1D) + H_2$ asymptote taken as zero.

dx.doi.org/10.1021/jp504411j | J. Phys. Chem. A 2014, 118, 4235−4242

and $2^1A'$) (left), and the vdW interaction regions could be recognized. It is clear that the contour lines are smooth and without any artificial oscillations in various regions. Compared with the old version of our PES, on which quantum wave packet calculations[30] are performed, the present PES could give a better description of CI and vdW regions.

Quasicalssical Trajectory Calculations. The QCT method has been described adequately in literature.[34,50,51] Here, we only give some details related to the present study. All the present QCT calculations are performed using a modified version of the VENUS96[52,53] code customized to incorporate our PES. For all the trajectories, the integration time step is 0.02 fs, which guarantees a conservation of the total energy better than 1 in 10^6. The trajectories are initiated at the C + H_2 asymptote with a separation of 8.0 Å between the two species and are terminated when the parting fragments reach the same separation, which is sufficiently large so that the interaction between the fragments is negligible. To fix the ZPE problem, a Gaussian function with the full-width-half-maximum (fwhm) of 0.1 is used as a weighting function in the GB approach.

The integral cross section (ICS) is evaluated using

$$\sigma_r = \pi b_{max}^2 \frac{1}{N_t} \sum_i^{N_r} w_i \tag{1}$$

where N_r is the reactive trajectory number, N_t is the total trajectory number, and w_i is the Gaussian weight for the ith reactive trajectory for the GB approach, which is set as 1 for all the reactive trajectories in the HB approach. The statistical uncertainty (68% confidence level) of the cross-section can be estimated by

$$\Delta\sigma_r = \pi b_{max}^2 \frac{1}{N_t}\left[\sum_i^{N_r} w_i^2 - \frac{1}{N_t}\left(\sum_i^{N_r} w_i\right)^2\right]^{1/2} \tag{2}$$

The differential cross section (DCS) is derived employing the method of moment expansion in Legendre polynomials.[34,54,55] The expressions are

$$\frac{d^2\sigma_r}{d\Omega} = \frac{\sigma_r}{2\pi} g(\cos\theta) = \frac{\sigma_r}{2\pi} \sum_{n=0}^{M} \frac{2n+1}{2} \langle P_n(\cos\theta)\rangle P_n(\cos\theta) \tag{3}$$

where $P_n(\cos\theta)$ is the n-degree Legendre polynomial, Ω is the solid angle (using the cylindrically symmetric $d\Omega = 2\pi \sin\theta\, d\theta$) and θ is the scattering angle, which is defined as the angle between the velocity vectors of the product H (or H_2) and the reactant H_2 in the center-of-mass system ($\theta = 0°$ is taken as the forward direction).

The statistical uncertainty[55] can be estimated by

$$\mathrm{var}\left[\frac{d^2\sigma_r}{d\Omega}\right] = \left(\sum_i^{N_r} w_i^2 / \left(\sum_i^{N_r} w_i\right)^2 - \frac{1}{N_t}\right)\left[\frac{d^2\sigma_r}{d\Omega}\right]^2 + \left(\frac{\sigma_R}{2\pi}\right)^2 \mathrm{var}[g(\cos\theta)] \tag{4}$$

with

$$\mathrm{var}[g(\cos\theta)] = \sum_{n=1}^{M} \gamma_n^2 P_n^2(\cos\theta) \tag{5}$$

$$\gamma_n^2 = \left(\sum_i^{N_r} w_i\right)^{-1}\left(\frac{2n+1}{2}\right)^2 [\langle P_n^2(\cos\theta)\rangle - \langle P_n(\cos\theta)\rangle^2] \tag{6}$$

The truncation of the polynomial series is addressed by performing the Smirnov–Kolmogorov test.[56] Significance levels higher than 94% can be achieved using four to 12 Legendre moments, ensuring good convergence, such that the inclusion of more terms does not produce any significant change.

When the relative translational energy E_{rel} is chosen from the Boltzmann distribution[57] at temperature T,

$$P(E_{rel}) = \frac{E_{rel}}{(k_B T)^2} \exp\left[-\frac{E_{rel}}{k_B T}\right] \tag{7}$$

A state-specific rate coefficient versus T is then obtained by integrating the cross section,

$$k_{vj}(T) = g_e\left(\frac{8k_B T}{\pi\mu}\right)^{1/2} \int_0^\infty \sigma(E_{rel})\, P(E_{rel})\, dE_{rel} = g_e\left(\frac{8k_B T}{\pi\mu}\right)^{1/2} \pi b_{max}^2 \frac{N_r}{N_t} \tag{8}$$

The thermal rate coefficient for the title reaction can be calculated from the expression

$$k(T) = g_e\left(\frac{8k_B T}{\pi\mu}\right)^{1/2} \sum_{vj} \frac{g_r(2j+1)\exp(-E_{vj}/k_B T)}{Q_{vj}} \times \int_0^\infty \sigma(E_{rel},v,j)\, P(E_{rel})\, dE_{rel} \tag{9}$$

where $g_e = 1/5$ is the electronic degeneracy factor, g_r is the ortho-para symmetry weight, k_B is the Boltzmann constant, μ is the reduced mass of the reactant species, E_{vj} is the rovibrational energy for the (v, j) state, Q_{vj} is the corresponding partition function, and $\sigma(E_{rel},v,j)$ is the reactive cross section.

In this paper, we perform the following QCT calculations. First, to obtain the cross sections at given collision energies, batches of 25 000–30 000 trajectories are calculated with b being sampled from $b = b_{max}\beta^{1/2}$ (β is a random number in the [0, 1] interval) and the initial H_2 molecule set on its ground rovibrational state ($v = 0$, $j = 0$). At each collision energy the maximum value of the impact parameter b_{max} is estimated by calculating batches of 3000 trajectories at fixed values of b and systematically increasing the value of b until no reactive trajectories are obtained. Second, with the aim of achieving the thermal rate coefficients for the temperature range of 200–1500 K, batches of 15 000–30 000 trajectories are calculated with b being sampled from $b = b_{max}\beta^{1/2}$ at each temperature and the value of b_{max} set to 7.0 Å, which is confirmed to be sufficient for collecting all the contributions to the reaction for various temperatures and rovibrational states of H_2. Moreover, the relative translational energy is randomly selected to mimic the Boltzmann distribution at the chosen temperature, and the initial H_2 molecule is set on different rovibrational states, which are related to all the contributions to the H_2 rovibrational Boltzmann distribution at the given temperature.

3. RESULTS AND DISCUSSION

Excitation Function. The excitation function (i.e., the ICS as a function of the collision energy) for the state-specific (v = 0, j = 0) C(^{1}D) + H_2 reaction is calculated in the collision

dx.doi.org/10.1021/jp504411j | J. Phys. Chem. A 2014, 118, 4235–4242

energy range from 0.01 to 0.5 eV, which is shown in Figure 2 and reported in Table 1. As illustrated in Figure 2, there is an initial sharp decline at low collision energies, whereas at high collision energies, the ICS curves level off gradually, which is consistent with the insertion mechanism. The same tendency is clearly displayed by the HB and GB results. It is quite obvious that the difference between the HB and GB ICSs is insignificant, only with the GB ICSs being a bit smaller than their HB counterparts.

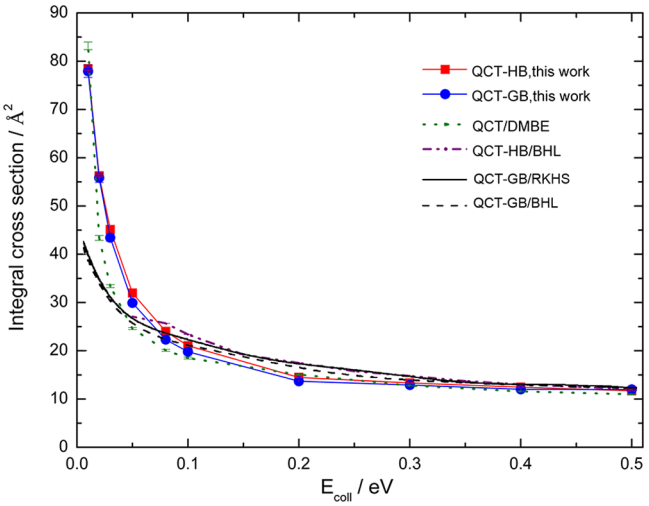

Figure 2. Excitation function for the $C(^1D) + H_2(v=0,j=0) \rightarrow CH + H$ reaction. The solid line with red squares displays the HB results, and the solid line with blue circles gives the GB results. Several previous theoretical results[18,26,29] are also presented.

Table 1. Integral Cross Section for the Reaction $C(^1D) + H_2(v=0,j=0)$

		$\sigma_r \pm \Delta\sigma_r$/Å^2		
E_{rel}/eV	b_{max}/Å	HB	GB	others
0.01	5.8	78.4 ± 0.3	77.9 ± 1.3	
0.02	5.1	56.3 ± 0.2	55.8 ± 1.0	
0.03	4.5	45.1 ± 0.2	44.4 ± 0.7	
0.05	3.9	32.0 ± 0.1	29.9 ± 0.5	
0.08	3.5	24.0 ± 0.1	22.3 ± 0.4	20.1,[a] 23.4,[b] 22.5,[c] 24.5,[d] 25.7[e]
0.1	3.3	21.1 ± 0.1	19.8 ± 0.4	
0.2	2.7	14.5 ± 0.1	13.7 ± 0.3	
0.3	2.5	13.3 ± 0.1	12.9 ± 0.2	
0.4	2.4	12.5 ± 0.1	12.0 ± 0.2	
0.5	2.3	11.7 ± 0.1	12.0 ± 0.2	

[a]Reference 29 QCT/DMBE. [b]Reference 18 QCT-GB/RKHS. [c]Reference 25 QCT-GB/BHL. [d]Reference 25 QCT-HB/BHL. [e]Reference 26 QCT-HB/BHL.

Figure 2 also shows a general good agreement between the present and previous QCT ICSs, though some differences can still be identified. At low collision energies, both the ICSs on the present and DMBE PESs decrease promptly with the increasing collision energy from very large initial values; this is a behavior typical of the barrierless insertion reactions, and contrasts with the less steep decline starting from a much lower ICS value obtained on the BHL or RKHS PES. As discussed in ref 29, this kind of difference may be attributed to the deficiencies of the BHL PES in the long-range part. We think that both the present and DMBE PESs have good descriptions of the long-range forces.

In addition, at the collision energies of 0.02−0.05 eV, the present ICSs are much larger than those on the DMBE PES. Because the same QCT method has been applied, the divergence is likely to result from the different topologies of the two PESs in the CI and vdW regions. As mentioned above, the location and energy of the CIs and vdW complexes in the entrance and exit valleys of our PES differ from those of the DMBE PES. The features of our new PES are in very good agreement with our high-level *ab initio* calculations.

Furthermore, we see from Table 1 that, at the collision energy of 0.08 eV, the present HB ICS has a value of 24.0 Å^2, which is larger than the QCT HB result of 20.1 Å^2 on the DMBE PES,[29] but a little smaller than the corresponding results of 24.5 and 25.7 Å^2 on the BHL PES.[25,26] Besides, the present GB ICS has a value of 22.7 Å^2, which is quite comparable to the previous QCT GB results of 23.2 Å^2 on the RKHS PES[18] and 22.5 Å^2 on the BHL PES.[25] However, at collision energies larger than 0.1 eV, the present GB ICSs are smaller than the results on the RKHS or BHL PESs, which can be explained by the evident differences of our PES and the BHL PES in the HCH CI regions. The present surface has a barrier with the height of 9.1 kcal/mol centered at the HCH linear geometry, which is much higher than that reported on the BHL PES (4.4 kcal/mol).[17] This barrier could hinder the bond fission close to the linear HCH CI and thus relatively smaller ICSs are obtained in this work.

Vibrational and Rotational Distributions of the CH Product. The vibrationally state-resolved integral cross sections and the product vibrational branching ratio that is defined as $\sigma(v'=1)/\sigma(v'=0)$ for the $C(^1D) + H_2$ $(v=0,j=0) \rightarrow H + CH(v',j')$ reaction calculated at different collision energies are presented in Figure 3. As can be seen, the state distribution is dominated by the ground vibrational state of CH for both the HB and GB results, and only a small fraction is distributed on the $v' = 1$ state, which is consistent with the experiments of Mikulecky et al.[10] Apparently, the ICSs ($v' = 0$) decrease as the collision energy increases for both HB and GB results, whereas for the ICSs ($v' = 1$), a different scenario is observed. The GB results tend to increase with the rise of the collision energy, whereas the HB results are lowered at first before ascending steadily. What's more worth mentioning is the comparison at the low collision energies, especially for the reaction yielding $CH(v'=1)$. In this case, the GB approach predicts a reaction threshold of 0.1 eV, whereas the HB results display no threshold. This is comprehensible because in the regular HB method, all the trajectories with v' being in the range from 0.5 to 1.5 are set as $v' = 1$. However, when the GB approach is employed, different weights are assigned to the trajectories, in such a way that the closer the v' value of a given trajectory is to the nearest integer, the larger is the weight of that trajectory. At the low collision energies below 0.1 eV, there are few trajectories with the v' values being close to 1, and therefore the overall cross section given by the GB approach is almost zero. This is consistent with the QCT-GB and QM calculations on the BHL PES, where a somewhat lower reaction threshold of 0.08 eV for the $CH(v'=1)$ channel has been predicted.[25]

As illustrated in Figure 3, the vibrational branching ratio increases with the collision energy for both the HB and GB results. However, the GB $\sigma(v'=1)/\sigma(v'=0)$ ratio is much lower than the HB ratio at low collision energies. For instance, the HB $\sigma(v'=1)/\sigma(v'=0)$ ratio at the collision energy of 0.08 eV is

dx.doi.org/10.1021/jp504411j | J. Phys. Chem. A 2014, 118, 4235−4242

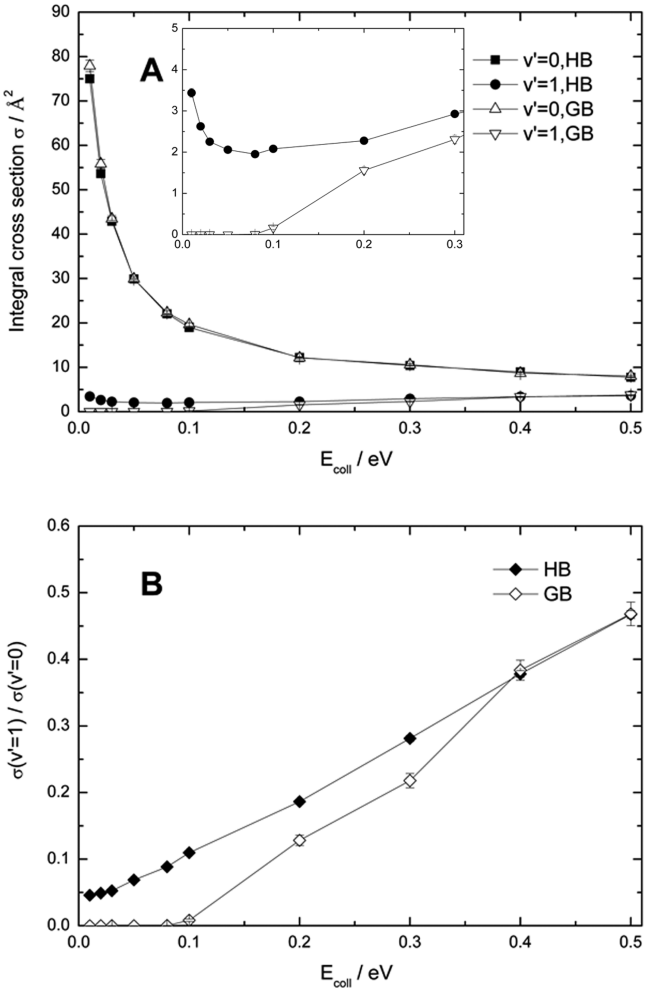

Figure 3. HB and GB results of (A) vibrationally state-resolved integral cross sections, where the inset is an amplified view of the low collision energy region, and (B) product vibrational branching ratio that is defined as $\sigma(v'=1)/\sigma(v'=0)$ as a function of collision energy.

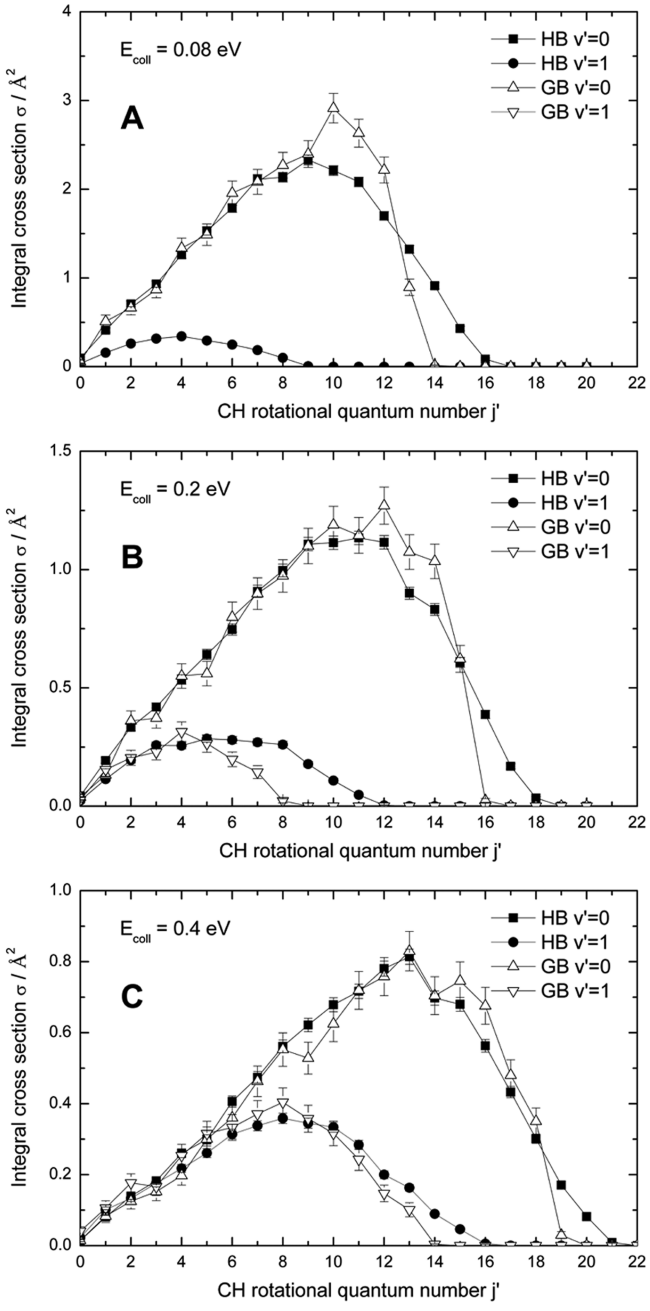

Figure 4. HB and GB results of the rotationally state-resolved integral cross sections calculated for the title reaction at (A) E_{coll} = 0.08 eV, (B) E_{coll} = 0.2 eV, and (C) E_{coll} = 0.4 eV.

0.088, whereas the GB ratio is almost 0. Our $\sigma(v'=1)/\sigma(v'=0)$ ratio is somewhat smaller than the corresponding value obtained from the QCT calculations using the BHL PES (0.12/0.011 for the HB/GB result, respectively).[25] These (particularly the GB results) are consistent with the experiment of Balucani et al.[14] at the same collision energy, in which the fraction of the product CH in the v' = 1 channel is too small to be determined. Furthermore, from Figure 3 we are able to deduce that the GB $\sigma(v'=1)/\sigma(v'=0)$ ratio at the collision energy of 0.17 eV (16 kJ/mol) is 0.08, which is consistent with the value of 0.098 from the QCT-GB calculations on the BHL PES and in good agreement with the approximate value of 0.04 obtained in the corresponding experiment.[14]

The rotationally state-resolved integral cross sections for the title reaction calculated at different collision energies are presented in Figure 4. As is depicted, the rotational state distribution is highly inverted and peaks near the highest accessible rotational state, which is consistent with the complex-forming mechanism. Both the HB and GB results suggest that the rotational state distribution becomes hot and the peaks shift to higher rotational states as the collision energy increases. At the collision energy of 0.08 eV, the difference in the shape of the rotational distributions between this work and the QCT calculations on the BHL surface is quite small.[25] The GB rotational distribution on the BHL surface for the CH(v'=0) channel shows a sharp peak at j' = 10−12, which is a little hotter than the present result (the GB rotational distribution peaks at j' = 10).

There is an overall good agreement between the HB and GB results. The shape of the GB rotational distribution for the CH(v'=0) state is well reproduced by the HB results, and the peaks are almost the same. However, some differences are visible. For instance, the HB results are hotter than the GB ones, especially at low collision energies. In particular, at the collision energy of 0.2 eV, the GB rotational state distribution for the CH(v'=0) state extends to a value of j' = 17, whereas the HB rotational state distribution reaches a larger value of j' = 19. For the CH(v'=1) channel, the GB rotational state

dx.doi.org/10.1021/jp504411j | J. Phys. Chem. A 2014, 118, 4235−4242

distribution only arrives at $j' = 9$, whereas the HB one extends to $j' = 12$. In addition, compared with the HB results, the GB rotationally state-resolved ICSs decrease more abruptly when the rotational quantum number j' approaches the maximum accessible j' value which is limited by the total available energy.

Differential Cross Sections. The DCSs calculated for the title reaction at different collision energies are presented in Figure 5. The difference between the HB and GB results is insignificant. As expected, both the HB and GB results are nearly forward−backward symmetric at all collision energies, which is consistent with the complex-forming mechanism. In addition, the polarization between forward/backward and sideways scattering seems to increase with the collision energy. This is understandable in light of the fact that at low collision energies, the collision complexes are on average much more long-lived, which will lead to an angular distribution more isotropic than that at high collision energies. A reasonable agreement is achieved between the QCT and experimental results at the collision energy of 0.08 eV.[14] However, the polarization between forward/backward and sideways scattering is larger in the QCT calculations than in the experiment, and this may primarily be ascribed to the contribution of the first excited singlet electronic state ($1^1A''$),[58,59] which is not taken into account in this work. Therefore, further exploration is anticipated.

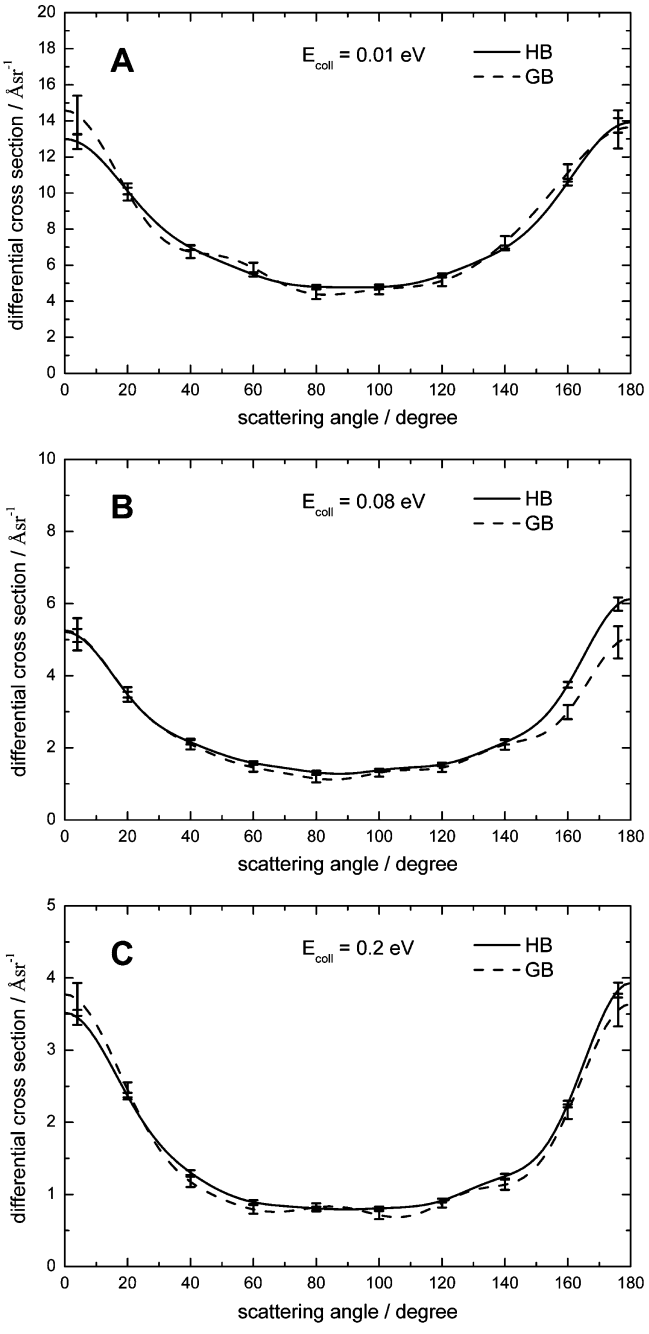

Figure 5. HB and GB results of the differential cross sections calculated for the title reaction at (A) E_{coll} = 0.01 eV, (B) E_{coll} = 0.08 eV, and (C) E_{coll} = 0.2 eV.

Thermal Rate Coefficients. The thermal rate coefficients for the $C(^1D) + H_2 \rightarrow CH + H$ reaction are calculated for the temperature range 200−1500 K with the QCT-HB approach, and the temperature dependence of thermal rate coefficients is shown in Figure 6. We see that the rate coefficients are nearly temperature-independent in the studied temperature range, which is consistent with the feature of the insertion mechanism. As expected from the comparison of the ICS results, our rate coefficients are larger than those computed on the DMBE surface over the whole temperature range, and we think that this results from different topologies of the two PESs in the CI and vdW regions. At room temperature, our value is $(1.54 \pm 0.03) \times 10^{-10}$ cm^3 molecule^{-1} s^{-1}, which is in very good agreement with the experimental value of $(2.0 \pm 0.6) \times 10^{-10}$ cm^3 molecule^{-1} s^{-1}.[12] It should be noted that the excited electronic state ($1^1A''$) and Renner-Teller effects may play some role in this reactive system.[60] However, as discussed in ref 61, the $1^1A''$ state makes a contribution of 30−40% to the total rate coefficients, so the overall thermal rate coefficients at the room temperature are estimated to range from 2.2×10^{-10} to 2.6×10^{-10} cm^3 molecule^{-1} s^{-1}, which are still within the experimental error limits.

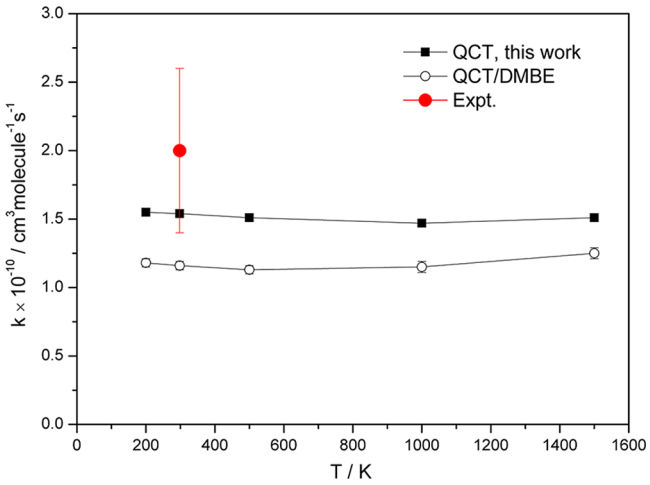

Figure 6. Temperature dependence of the thermal rate coefficients for the title reaction. The solid line with circles displays the QCT results on the DMBE surface,[29] and the solid red circle denotes the experimental value.[12]

4. CONCLUSIONS

We have performed detailed QCT studies on a new global *ab initio* PES for the singlet ground state ($1^1A'$) of the C + H_2 reactive system. Various dynamical quantities are investigated in

dx.doi.org/10.1021/jp504411j | J. Phys. Chem. A 2014, 118, 4235−4242

a wide range of collision energies. The excitation function is reported and the obtained ICSs are much larger than the previous QCT results at low collision energies, which can be attributed to the improvement of our PES in the CI and vdW regions. The DCS is dominated by the scattering in both the forward and backward directions with almost forward–backward symmetry, which is consistent with experiment. The rotational state distribution of the CH product is highly inverted and peaks near the highest accessible rotational state, whereas the vibrational state distribution of the CH product peaks strongly at the ground vibrational state, which is in very good agreement with experiment. These observations are consistent with the complex-forming mechanism. Furthermore, the thermal rate coefficients for the temperature range 200–1500 K have been obtained, and it is encouraging to see that our QCT rate coefficients agree with the available experimental data very well, reflecting the accuracy of the present PES. It will be a topic of our future research to study the role of the first excited singlet electronic state ($1^1A''$) in the title reaction.

AUTHOR INFORMATION

Corresponding Authors

*J. Cao: e-mail, caojw@iccas.ac.cn.

*W. Bian: e-mail, bian@iccas.ac.cn.

Notes

The authors declare no competing financial interest.

ACKNOWLEDGMENTS

This work is supported by the Chinese Ministry of Science and Technology (No. 2013CB834601), the National Natural Science Foundation of China (Nos. 21173232, 91221105, 21303217), and ICCAS (Institute of Chemistry, Chinese Academy of Sciences) (No. CMS-PY-201332). Many computations are carried out at Virtual Laboratory of Computational Chemistry, Computer Network Information Center of Chinese Academy of Sciences.

REFERENCES

(1) Skell, P. S.; Havel, J. J.; McGlinchey, M. J. Chemistry and the Carbon Arc. *Acc. Chem. Res.* **1973**, *6*, 97–105.

(2) Liu, K. Excitation Functions of Elementary Chemical Reactions: A Direct Link From Crossed-Beam Dynamics to Thermal Kinetics ? *Int. Rev. Phys. Chem.* **2001**, *20*, 189–217.

(3) Guo, H. Quantum Dynamics of Complex-Forming Bimolecular Reactions. *Int. Rev. Phys. Chem.* **2012**, *31*, 1–68.

(4) Aoiz, F. J.; Bañares, L.; Herrero, V. J. Dynamics of Insertion Reactions of H_2 Molecules with Excited Atoms. *J. Phys. Chem. A* **2006**, *110*, 12546–12565.

(5) González-Lezana, T. Statistical Quantum Studies on Insertion Atom–Diatom Reactions. *Int. Rev. Phys. Chem.* **2007**, *26*, 29–91.

(6) Casavecchia, P. Chemical Reaction Dynamics with Molecular Beams. *Rep. Prog. Phys.* **2000**, *63*, 355–414.

(7) Jursich, G. M.; Wiesenfeld, J. R. Product Energetics of the Reaction $C(^1D) + H_2 \rightarrow CH + H$. *Chem. Phys. Lett.* **1984**, *110*, 14–19.

(8) Fisher, W. H.; Carrington, T.; Sadowski, C. M.; Dugan, C. H. The Reactions of C (2^1D_2) with H_2, D_2 and HD: Product Rotational Energies, Isotope Effects and the CD/CH Branching Ratio. *Chem. Phys.* **1985**, *97*, 433–448.

(9) Scott, D. C.; de Juan, J.; Robie, D. C.; Schwartz-Lavi, D.; Reisler, H. Reactions of $C(^1D)$ with H_2 and HCl: Product State Excitations, Λ-Doublet Propensities, and Branching Ratios. *J. Phys. Chem.* **1992**, *96*, 2509–2518.

(10) Mikulecky, K.; Gericke, K.-H. Reaction Dynamics of $C(^1D) + H_2$ (v) $\rightarrow$ CH ($X^2\prod$) + H. *J. Chem. Phys.* **1993**, *98*, 1244–1251.

(11) Scholefield, M. R.; Goyal, S.; Choi, J.-H.; Reisler, H. Reactions of Hyperthermal $C(^3P)$ Generated by Laser Ablation with H_2, HCl, HBr, and CH_3OH. *J. Phys. Chem.* **1995**, *99*, 14605–14613.

(12) Sato, K.; Ishida, N.; Kurakata, T.; Iwasaki, A.; Tsuneyuki, S. Reactions of $C(^1D)$ with H_2, HD and D_2: Kinetic Isotope Effect and the CD/CH Branching Ratio. *Chem. Phys.* **1998**, *237*, 195–204.

(13) Bergeat, A.; Cartechini, L.; Balucani, N.; Capozza, G.; Philips, L. F.; Casavecchia, P. G.; Volpi, G.; Bonnet, L.; Rayez, J.-C. A Crossed-Beam Study of the Reaction C (^1D) + H_2 ($X^1\Sigma^+$, $v = 0$) $\rightarrow$ CH ($X^2\Pi$, v') + H(^2S). *Chem. Phys. Lett.* **2000**, *327*, 197–202.

(14) Balucani, N.; Capozza, G.; Cartechini, L.; Bergeat, A.; Bobbenkamp, R.; Casavecchia, P.; Aoiz, F. J.; Bañares, L.; Honvault, P.; Bussery-Honvault, B.; et al. Dynamics of the Insertion Reaction $C(^1D) + H_2$: A Comparison of Crossed Molecular Beam Experiments with Quasiclassical Trajectory and Quantum Mechanical Scattering Calculations. *Phys. Chem. Chem. Phys.* **2004**, *6*, 4957–4967.

(15) Balucani, N.; Casavecchia, P.; Aoiz, F. J.; Bañares, L.; Launay, J.-M.; Bussery-Honvault, B.; Honvault, P. Dynamics of the $C(^1D)+H_2$ Reaction: A Comparison of Crossed Molecular Beam Experiments with Quantum Mechanical and Quasiclassical Trajectory Calculations on the First Two Singlet ($1^1A'$ and $1^1A''$) Potential Energy Surfaces. *Mol. Phys.* **2010**, *108*, 373–380.

(16) Balucani, N.; Capozza, G.; Segoloni, E.; Bobbenkamp, R.; Casaveechia, P.; Gonzalez-Lezana, T.; Rackham, E. J.; Bañares, L.; Aoiz, F. J. Dynamics of the $C(^1D) + D_2$ Reaction: A Comparison of Crossed Molecular-Beam Experiments with Quasiclassical Trajectory and Accurate Statistical Calculations. *J. Chem. Phys.* **2005**, *122*, 234309/1–11.

(17) Busery-Honvault, B.; Honvault, P.; Launay, J.-M. A Study of the $C(^1D) + H_2 \rightarrow CH + H$ Reaction: Global Potential Energy Surface and Quantum Dynamics. *J. Chem. Phys.* **2001**, *115*, 10701–10708.

(18) Bañares, L.; Aoiz, F. J.; Vázquez, S. A.; Ho, T.-S.; Rabitz, H. Quasi-Classical Trajectory Calculations on a Fast Analytic Potential Energy Surface for the $C(^1D) + H_2$ Reaction. *Chem. Phys. Lett.* **2003**, *374*, 243–251.

(19) Defazio, P.; Petrongolo, C.; Bussery-Honvault, B.; Honvault, P. Born–Oppenheimer Quantum Dynamics of the $C(^1D) + H_2$ Reaction on the CH_2 $\tilde{a}^1A_1$ and $\tilde{b}^1B_1$ Surfaces. *J. Chem. Phys.* **2009**, *131*, 114303/1–6.

(20) Rackham, E. J.; Gonzalez-Lezana, T.; Manolopoulos, D. E. A Rigorous Test of the Statistical Model for Atom–Diatom Insertion Reactions. *J. Chem. Phys.* **2003**, *119*, 12895–12907.

(21) Lin, S. Y.; Guo, H. Quantum Wave Packet Studies of the $C(^1D) + H_2 \rightarrow CH + H$ Reaction: Integral Cross Section and Rate Constant. *J. Phys. Chem. A* **2004**, *108*, 2141–2148.

(22) Lin, S. Y.; Guo, H. Case Study of a Prototypical Elementary Insertion Reaction: $C(^1D) + H_2 \rightarrow CH + H$. *J. Phys. Chem. A* **2004**, *108*, 10066–10071.

(23) Liu, J.; Fu, B.; Zhang, D. Quantum Wave Packet Study of the $C(^1D) + H_2$ Reaction. *Chem. Phys. Lett.* **2009**, *480*, 46–48.

(24) Honvault, P.; Bussery-Honvault, B.; Launay, J.-M.; Aoiz, F. J.; Bañares, L. Quantum Mechanical and Quasiclassical Trajectory Scattering Calculations for the $C(^1D) + H_2$ Reaction on the Second Excited $1^1A''$ Potential Energy Surface. *J. Chem. Phys.* **2006**, *124*, 154314/1–7.

(25) Bañares, L.; Aoiz, F. J.; Honvault, P.; Bussery-Honvault, B.; Launay, J.-M. Quantum Mechanical and Quasi-Classical Trajectory Study of the $C(^1D) + H_2$ Reaction Dynamics. *J. Chem. Phys.* **2003**, *118*, 565–568.

(26) Kang, L. H.; Dai, B. Effect of Collision Energy on Cross Sections and Product Alignments for the $C(^1D) + H_2$ ($v = 0$, $j = 0$) Insertion Reactions. *Can. J. Chem.* **2010**, *88*, 453–457.

(27) Aoiz, F. J.; González-Lezana, T.; Rábanos, V. S. A Comparison of Quantum and Quasiclassical Statistical Models for Reactions of Electronically Excited Atoms with Molecular Hydrogen. *J. Chem. Phys.* **2008**, *129*, 094305/1–12.

(28) Joseph, S.; Varandas, A. J. C. Accurate Double Many-Body Expansion Potential Energy Surface for the Lowest Singlet State of Methylene. *J. Phys. Chem. A* **2009**, *113*, 4175–4183.

(29) Joseph, S.; Caridade, P. J. S. B.; Varandas, A. J. C. Quasiclassical Trajectory Study of the C(^{1}D) + H_2 Reaction and Isotopomeric Variants: Kinetic Isotope Effect and CD/CH Branching Ratio. *J. Phys. Chem. A* **2011**, *115*, 7882−7890.
(30) Sun, Z.; Zhang, C.; Lin, S.; Zheng, Y.; Meng, Q.; Bian, W. Quantum Reaction Dynamics of the C(^{1}D) + H_2(D_2) → CH(D) + H(D) on a New Potential Energy Surface. *J. Chem. Phys.* **2013**, *139*, 014306/1−6.
(31) Greaves, S. J.; Wrede, E.; Goldberg, N. J.; Zhang, J.; Miller, D. J.; Zare, R. N. Vibrational Excitation through Tug-of-War Inelastic Collisions. *Nature* **2008**, *454*, 88−91.
(32) Cao, J.; Zhang, Z.; Zhang, C.; Liu, K.; Wang, M.; Bian, W. Quasiclassical Trajectory Study of H + SiH_4 Reactions in Full-Dimensionality Reveals Atomic-Level Mechanisms. *Proc. Natl. Acad. Sci. U. S. A.* **2009**, *106*, 13180−13185.
(33) Czakó, G.; Bowman, J. M. Dynamics of the Reaction of Methane with Chlorine Atom on an Accurate Potential Energy Surface. *Science* **2011**, *334*, 343−346.
(34) Aoiz, F. J.; Bañares, L.; Herrero, V. J. Recent Results from Quasiclassical Trajectory Computations of Elementary Chemical Reactions. *J. Chem. Soc., Faraday Trans.* **1998**, *94*, 2483−2500.
(35) Bonnet, L.; Rayez, J.-C. Quasiclassical Trajectory Method for Molecular Scattering Processes: Necessity of a Weighted Binning Approach. *Chem. Phys. Lett.* **1997**, *277*, 183−190.
(36) Bonnet, L.; Rayez, J.-C. Gaussian Weighting in the Quasiclassical Trajectory Method. *Chem. Phys. Lett.* **2004**, *397*, 106−109.
(37) Varandas, A. J. C. Trajectory Binning Scheme and Non-active Treatment of Zero-point Energy Leakage in Quasi-classical Dynamics. *Chem. Phys. Lett.* **2007**, *439*, 386−392.
(38) Knowles, P. J.; Werner, H.-J. An Efficient Method for the Evaluation of Coupling Coefficients in Configuration Interaction Calculations. *Chem. Phys. Lett.* **1988**, *145*, 514−522.
(39) Werner, H.-J.; Knowles, P. J. An Efficient Internally Contracted Multiconfiguration-Reference Configuration Interaction Method. *J. Chem. Phys.* **1988**, *89*, 5803−5814.
(40) Werner, H.-J.; Knowles, P. J.; Knizia, G.; Manby, F. R.; Schütz, M.; Lindh, R.; et al. *MOLPRO*, version 2012.1, a package of ab initio programs. http://www.molpro.net.
(41) Dunning, J. T. H. Gaussian Basis Sets for Use in Correlated Molecular Calculations. I. The Atoms Boron through Neon and Hydrogen. *J. Chem. Phys.* **1989**, *90*, 1007−1023.
(42) Kendall, R. A.; Dunning, T. H.; Harrison, R. J. Electron Affinities of the First-Row Atoms Revisited. Systematic Basis Sets and Wave Functions. *J. Chem. Phys.* **1992**, *96*, 6796−6806.
(43) Murrell, J. N.; Carter, S.; Farantos, S. C.; Huxley, P.; Varandas, A. J. C. *Molecular Potential Energy Functions*; Wiley: New York, 1984.
(44) Varandas, A. J. C. Intermolecular and Intramolecular Potentials: Topographical Aspects, Calculation, and Functional Representation via A Double Many-Body Expansion Method. *Adv. Chem. Phys.* **1988**, *74*, 255−338.
(45) Ma, H.; Zhang, C.; Zhang, Z.; Liu, X.; Bian, W. New Ab Initio Potential Energy Surfaces for the Renner-Teller Coupled $1^1A'$ and $1^1A''$ States of CH_2. *Adv. Phys. Chem.* **2012**, *2012*, 236750/1−12.
(46) Bian, W.; Werner, H.-J. Global Ab Initio Potential Energy Surfaces for the ClH_2 Reactive System. *J. Chem. Phys.* **2000**, *112*, 220−229.
(47) Skouteris, D.; Manolopoulos, D.; Bian, W.; Werner, H.-J.; Lai, L.; Liu, K. van der Waals Interactions in the Cl + HD Reaction. *Science* **1999**, *286*, 1713−1716.
(48) Aguado, A.; Paniagua, M. A New Functional Form to Obtain Analytical Potentials of Triatomic Molecules. *J. Chem. Phys.* **1992**, *96*, 1265−1275.
(49) Zhang, C.; Fu, M.; Shen, Z.; Ma, H.; Bian, W. Global Analytical ab initio Ground-State Potential Energy Surface for the C(^{1}D)+H_2 Reactive System. *J. Chem. Phys.* **2014**, DOI: 10.1063/1.4881896.
(50) Sewell, T. D.; Thompson, D. L. Classical Trajectory Methods for Polyatomic Molecules. *Int. J. Mod. Phys. B* **1997**, *11*, 1067−1112.
(51) Peslherbe, G. H.; Wang, H.; Hase, W. L. Monte Carlo Sampling for Classical Trajectory Simulations. *Adv. Chem. Phys.* **1999**, *105*, 171−201.
(52) Hase, W. L.; Duchovic, R. J.; Hu, X.; Komornicki, A.; Lim, K. F.; Lu, D.-H.; Peslherbe, G. H.; Swamy, K. N.; Linde, S. R. V.; Varandas, A. *VENUS96: A General Chemical Dynamics Computer Program*; Bulletin Number 16 of the Quantum Chemistry Program Exchange; Indiana University: Bloomington, IN, 1996; p 671.
(53) Hu, X.; Hase, W. L.; Pirraglia, T. Vectorization of the General Monte Carlo Classical Trajectory Program VENUS. *J. Comput. Chem.* **1991**, *12*, 1014−1024.
(54) Aoiz, F. J.; Herrero, V. J.; Rábanos, V. S. Effects of Translational, Rotational, and Vibrational Energy on the Dynamics of the D + H_2 Exchange Reaction. A Classical Trajectory Study. *J. Chem. Phys.* **1991**, *94*, 7991−8007.
(55) Aoiz, F. J.; Herrero, V. J.; Rábanos, V. S. Quasiclassical State to State Reaction Cross Sections for D + H_2 (v = 0, j = 0) → HD (v', j') +H. Formation and Characteristics of Short-Lived Collision Complexes. *J. Chem. Phys.* **1992**, *97*, 7423−7436.
(56) Press, W. H.; Teukolsky, S. A.; Vetterling, W. T.; Flannery, B. P. *Numerical Recipes in Fortran77*; Cambridge University Press: Cambridge, U.K., 1992.
(57) Porter, R. N.; Raff, L. M. In *Dynamics of Molecular Collisions, Part B*; Miller, W. H., Ed.; Plenum Press: New York, 1976.
(58) Green, W. H.; Handy, N. C.; Knowles, P. J.; Carter, S. Theoretical Assignment of the Visible Spectrum of Singlet Methylene. *J. Chem. Phys.* **1991**, *94*, 118−132.
(59) Liu, X.; Bian, W.; Zhao, X.; Tao, X. Potential Energy Surface Intersections in the C(^{1}D)H_2 Reactive System. *J. Chem. Phys.* **2006**, *125*, 074306/1−7.
(60) Zhang, Z.; Ma, H.; Bian, W. Accurate Quantum Mechanical Study of the Renner-Teller Effect in the Singlet CH_2. *J. Chem. Phys.* **2011**, *135*, 154303/1−10.
(61) Defazio, P.; Gamallo, P.; González, M.; Akpinar, S.; Bussery-Honvault, B.; Honvault, P.; Petrongolo, C. Quantum Dynamics of the C(^{1}D) + HD and C(^{1}D) + n−D_2 Reactions on the $\tilde{a}^1A'$ and $\tilde{b}^1A''$ Surfaces. *J. Chem. Phys.* **2010**, *132*, 104306/1−8.